

Journal Pre-proof

Physical-biological drivers modulating phytoplankton seasonal succession along the Northern Antarctic Peninsula

Raul Rodrigo Costa, Afonso Ferreira, Márcio S. de Souza, Virginia M. Tavano, Rodrigo Kerr, Eduardo R. Secchi, Vanda Brotas, Tiago S. Dotto, Ana C. Brito, Carlos R.B. Mendes

PII: S0013-9351(23)01077-0

DOI: <https://doi.org/10.1016/j.envres.2023.116273>

Reference: YENRS 116273

To appear in: *Environmental Research*

Received Date: 22 February 2023

Revised Date: 18 May 2023

Accepted Date: 27 May 2023

Please cite this article as: Costa, R.R., Ferreira, A., de Souza, Má.S., Tavano, V.M., Kerr, R., Secchi, E.R., Brotas, V., Dotto, T.S., Brito, A.C., Mendes, C.R.B., Physical-biological drivers modulating phytoplankton seasonal succession along the Northern Antarctic Peninsula, *Environmental Research* (2023), doi: <https://doi.org/10.1016/j.envres.2023.116273>.

This is a PDF file of an article that has undergone enhancements after acceptance, such as the addition of a cover page and metadata, and formatting for readability, but it is not yet the definitive version of record. This version will undergo additional copyediting, typesetting and review before it is published in its final form, but we are providing this version to give early visibility of the article. Please note that, during the production process, errors may be discovered which could affect the content, and all legal disclaimers that apply to the journal pertain.

© 2023 Published by Elsevier Inc.



R.R.C. and C.R.B.M. contributed to the conception and design of this work. C.R.B.M., M.S.S and R.K. carried out the collection of in situ data. R.R.C. and C.R.B.M. carried out the HPLC/CHEMTAX analyses. R.R.C. and A.F. performed the remote sensing analysis. T.S.D. performed the physical oceanography analysis. M.S.S. carried out the macroscopy analysis. R.R.C. wrote the first draft of the manuscript and developed the figures. A.F., M.S.S., R.K., T.S.D., V.M.T, A.C.B, V.B., E.S. and C.R.B.M contributed to the organization and writing of the final version of the manuscript. All authors contributed to manuscript revision, read, and approved the submitted version.

1 **Physical-biological drivers modulating phytoplankton seasonal**
2 **succession along the Northern Antarctic Peninsula**

3 Raul Rodrigo Costa^{1,2*}; Afonso Ferreira^{1,3}; Márcio S. de Souza^{1,2}; Virginia M.
4 Tavano¹; Rodrigo Kerr¹; Eduardo R. Secchi^{1,2}; Vanda Brotas³; Tiago S. Dotto⁴;
5 Ana C. Brito³ & Carlos R. B. Mendes^{1,2}

6

7

8 ¹Instituto de Oceanografia, Universidade Federal do Rio Grande (FURG), Av.
9 Itália, km 8, Rio Grande, RS 96203-900, Brazil.

10 ²Programa de Pós-graduação em Oceanografia Biológica, Universidade Federal
11 do Rio Grande (FURG), Rio Grande, RS 96203-900, Brazil.

12 ³MARE – Centro de Ciências do Mar e do Ambiente, Faculdade de Ciências,
13 Universidade de Lisboa, Campo Grande, 1749-016 Lisboa, Portugal.

14 ⁴Ocean and Earth Science, University of Southampton, National Oceanography
15 Centre, Southampton, UK.

16

17

18 *Corresponding author: Tel. + 55 53 3233 6535; E-mail address: costa@furg.br
19 (R. R. Costa).

20

21

22

23

24 **Abstract**

25 The Northern Antarctic Peninsula (NAP) shows shifts in phytoplankton
26 distribution and composition along its warming marine ecosystems. However,
27 despite recent efforts to mechanistically understand these changes, little focus
28 has been given to the phytoplankton seasonal succession, remaining
29 uncertainties regarding to distribution patterns of emerging taxa along the NAP.
30 To fill this gap, we collected phytoplankton (pigment and microscopy analysis)
31 and physico-chemical datasets during spring and summer (November, February
32 and March) of 2013/2014 and 2014/2015 off the NAP. Satellite measurements
33 (sea surface temperature, sea ice concentration and chlorophyll-*a*) were used to
34 extend the temporal coverage of analysis associated with the *in situ* sampling.
35 We improved the quantification and distribution pattern of emerging taxa, such
36 as dinoflagellates and cryptophytes, and described a contrasting seasonal
37 behavior and distinct fundamental niche between centric and pennate diatoms.
38 Cryptophytes and pennate diatoms preferentially occupied relatively shallower
39 mixing layers compared with centric diatoms and dinoflagellates, suggesting
40 differences between these groups in distribution and environment occupation
41 over the phytoplankton seasonal succession. Under colder conditions, negative
42 sea surface temperature anomalies were associated with positive anomalies of
43 sea ice concentration and duration. Therefore, based on sea ice–phytoplankton
44 growth relationship, large phytoplankton biomass accumulation was expected
45 during the spring/summer of 2013/2014 and 2014/2015 along the NAP. However,
46 there was a decoupling between sea ice concentration/duration and
47 phytoplankton biomass, characterizing two seasonal periods of low biomass
48 accumulation (negative chlorophyll-*a* anomalies), associated with the top-down

49 control in the region. These results provide an improved mechanistic
50 understanding on physical-biological drivers modulating phytoplankton seasonal
51 succession along the Antarctic coastal waters.

52

53 **Keywords:** Climate change, Southern Ocean, upper ocean physical structures,
54 top-down control, phytoplankton taxa, shifts.

55

56 **Introduction**

57 The sea ice retreat-driven melting allows upper ocean stratification during
58 spring/summer, leading to favorable sunlight conditions for phytoplankton
59 biomass accumulation along the Southern Ocean (Ducklow et al. 2013). In
60 general, small cells dominate the phytoplankton community structure during
61 spring as large cells develop to form blooms in summer months (Petrou et al.
62 2016). The Southern Ocean is known as a bottom-up control complex system
63 characterized by a tight trophic coupling (Saba et al. 2014). Spring/summer
64 positive chlorophyll-*a* (Chl-*a*; an index of phytoplankton biomass) anomalies are
65 associated with an increased previous winter sea ice extent and duration, being
66 related to robust cohorts of krill on the following summer season after
67 phytoplankton bloom events (Ducklow et al. 2013, Saba et al. 2014). This makes
68 the dynamic of phytoplankton seasonal succession along the Southern Ocean,
69 since the initial growth to senescence stage of cells, a link between physico-
70 chemical processes and higher trophic levels, with important implications to

71 energy flux through food webs and biogeochemical cycles (Saba et al. 2014;
72 Petrou et al. 2016; Santos-Andrade et al. 2023).

73 Due to a poleward warming in the past decades (Henley et al. 2019),
74 changes in sea ice season have raised uncertainties regarding the phytoplankton
75 seasonal succession and warming-driven species response off the Southern
76 Ocean (Petrou et al. 2016; Ferreira et al. 2020). One example is the West
77 Antarctic Peninsula (WAP), which has been undergoing critical physical changes
78 in its marine ecosystems (Henley et al. 2019). While there has been a short-term
79 plateau from the late 1990s, WAP long-term trends (since the mid-20th century)
80 of winter atmospheric warming and reduced sea ice season remain statistically
81 significant (Henley et al. 2019). Mid-ocean warming-induced glacier retreat has
82 also been recorded (Cook et al. 2016). These long-term physical changes along
83 the WAP due to its north-south orientation have caused a marked meridional
84 difference on biological compartments, especially at the base of the food-web
85 (Montes-Hugo et al. 2009; Ducklow et al. 2013).

86 The mid/southern WAP shows a dry polar system, with an increased
87 southward phytoplankton biomass, while a warmer maritime condition has been
88 recorded along the northern WAP (hereafter Northern Antarctic Peninsula; NAP),
89 associated with a decreased phytoplankton biomass in the past decades
90 (Montes-Hugo et al. 2009; Ferreira et al. 2020). In a warming NAP, decreased
91 phytoplankton biomass has been associated with a decreased proportion of large
92 centric diatoms, which have been replaced by small nanoflagellate cells linked
93 with increasingly meltwater input (Montes-Hugo et al. 2009; Costa et al. 2021;
94 Mendes et al. 2023). These previous results indicate climate change impacts at

95 the base of the food web with a myriad of cascading effects across all higher
96 trophic levels off the NAP (Ferreira et al. 2020). However, there is a generalized
97 understanding about climate change effects on diatom functional group along the
98 region (Montes-Hugo et al. 2009). For instance, few studies have evaluated
99 distribution patterns and biomass accumulation of pennate diatoms, remaining
100 uncertainties on their plasticity and adaptation to cope with the reported
101 ecosystem changes (Petrou et al. 2016).

102 Although seasonal succession studies on phytoplankton community
103 composition have been conducted along the WAP, they typically focus on the
104 mid/southern WAP (e.g., Garibotti et al. 2005; Rozema et al. 2017; Schofield et
105 al. 2017), where a dry polar system is persistent, and/or on punctual stations,
106 encompassing only a limited sampling area along the NAP (Rodriguez et al. 2002;
107 Varela et al. 2002; Pan et al. 2020). These spatial/temporal constraints prevent
108 to assess phytoplankton community composition under different seasonal drivers
109 along the NAP, limiting the current knowledge regarding to succession and
110 distribution patterns of emerging taxa, such as dinoflagellates (Ferreira et al.
111 2020; Mascioni et al. 2021). To fill this gap, we collected phytoplankton (pigment
112 and microscopy analysis) and physico-chemical (salinity, temperature and
113 macronutrients) datasets along a large oceanic area of the NAP during two
114 consecutive spring/summer Antarctic expeditions between 2013/2014 and
115 2014/2015. Additionally, remote sensing measurements were used to extend the
116 temporal coverage of analysis associated with the *in situ* sampling. We also
117 applied generalized linear models to quantitatively describe environmental
118 parameters modulating phytoplankton biomass accumulation during the seasonal
119 succession periods along the NAP.

120

121 **Methods**

122 **Sample collection.** The NAP marine region, which includes the Gerlache and
123 Bransfield Straits, the northwestern Weddell Sea, and the southernmost part of
124 the Drake Passage, is a complex system characterized by distinct hydrography
125 features (Ferreira et al. 2020). Due to north-south contrasting oceanographic
126 properties along the NAP, the sampling grid in this study was split in two
127 subregions: north and south (Fig. 1a), which delimited the areas used to estimate
128 average remote sensing measurements (Fig. 1b,c,d). The study area covered
129 from the Gerlache and Bransfield Straits to the proximity of Elephant Island (Fig.
130 1). Data were collected during six seasonal oceanographic cruises conducted on
131 board the *NPo Almirante Maximiano* of the Brazilian Navy between November
132 2013 and March 2015 along the NAP (Fig. 1). The cruises were conducted during
133 the late spring (November 2013 and 2014) and mid/late summer (February 2014
134 and 2015 and March 2014 and 2015). Moreover, we used an additional dataset
135 sampled at the same area during the spring/summer (November and February,
136 respectively) of 2015/2016 along the NAP (Costa et al. 2021). This previous
137 published dataset of 2015/2016 is used in this present study as a baseline, given
138 the high Chl-*a* anomaly recorded (Costa et al. 2021), to compare with the physical
139 parameters measured during the spring/summer of 2013/2014 and 2014/2015
140 (see Fig. 1 and Supplementary Figs. 5 and 6). We assume, disregarding
141 interspecific differences, that physical parameters (e.g., salinity, temperature, sea
142 ice concentration and mixed layer depth) during the 2015/2016 spring/summer
143 were close to ideal for phytoplankton biomass accumulation ($> 45 \text{ mg m}^{-3} \text{ Chl-}a$).

144 A combined Sea-Bird CTD (conductivity–temperature–depth
145 instrument)/Carrousel 911+system[®] equipped with 24 five-litre Niskin bottles was
146 used to measure the hydrographic data profiles, such as *in situ* temperature (°C)
147 and practical salinity. Along with CTD measurements, seawater samples were
148 collected at surface (5 m) using Niskin bottles to perform phytoplankton and
149 macronutrient analysis. Seawater samples (0.5–2.5 L) were filtered under low
150 vacuum through GF/F (0.7 µm pore size) and cellulose acetate membrane (0.45
151 µm pore size) filters to phytoplankton and dissolved inorganic macronutrient
152 analysis, respectively. Size fractionation of phytoplankton biomass (mg m⁻³ Chl-
153 a) was also performed through sequential filtering of surface seawater samples
154 (see Costa et al. 2021 for further details), yielding measurements of Chl-a (mg
155 m⁻³) concentration to the pico-(0.7–2 µm), nano- (2–20 µm) and micro-
156 phytoplankton (> 20 µm). The filters were frozen in liquid nitrogen for later
157 HPLC/CHEMTAX analysis. Additionally, surface seawater samples were also
158 preserved to microscopy analysis in amber glass flasks (±250 mL) with 2%
159 alkaline Lugol's iodine solution.

160

161 **Physico-chemical measurements.** Seawater thermodynamic calculations were
162 performed with the Thermodynamic Equation of Seawater – 2010 (TEOS–10).
163 For each CTD cast, the seawater potential density (kg m⁻³) referenced to 0 dbar
164 was determined based on seawater conservative temperature, absolute salinity
165 and pressure data. To examine the water column physical structure, mixed layer
166 depth (MLD; m) was calculated as the depth at which seawater potential density
167 deviates from its 10 m depth value by a threshold of 0.03 kg m⁻³ (de Boyer
168 Montégut et al. 2004). Dissolved inorganic nitrogen (DIN – nitrate, nitrite and

169 ammonium), phosphate and silicic acid (silicate) were measured following the
170 spectrophotometric determination methods described by Aminot and
171 Chaussepied (1983) with an accuracy around $\pm 5\%$ for all analysed
172 macronutrients. Detection limits were $0.11 \mu\text{M}$ for DIN, $0.10 \mu\text{M}$ for phosphate
173 and $0.5 \mu\text{M}$ for silicic acid.

174

175 **Phytoplankton analysis.** The concentrations of Chl-*a* and class-specific
176 accessory pigments were measured by High Performance Liquid
177 Chromatography (HPLC). In the laboratory, the filters were placed in a screw cap
178 centrifuge tube with 3 mL of 95% cold-buffered methanol (2% ammonium
179 acetate) containing 0.05 mg L^{-1} trans- β -apo-8'-carotenal (Fluka) as internal
180 standard. Samples were sonicated for 5 min in an ice-water bath, placed at -20°C
181 for 1 h, and then centrifuged at 1100 g for 5 min at 3°C . The supernatants were
182 filtered through Fluoropore PTFE membrane filters ($0.2 \mu\text{m}$ pore size) to separate
183 the extract from remains of filter and cell debris. Immediately prior to injection,
184 $1000 \mu\text{L}$ of sample were mixed with $400 \mu\text{L}$ of Milli-Q water in 2.0-mL amber glass
185 sample vials, which then were placed in the HPLC cooling rack (4°C). The
186 pigment extracts were analysed using a Shimadzu HPLC constituted by a solvent
187 distributor module (LC-20 AD) with a control system (CBM-20A), a photodiode
188 detector (SPDM20A) and a fluorescence detector (RF-10AXL). The
189 chromatographic separation of the pigments was performed using a monomeric
190 C8 column (SunFire; 15 cm long; 4.6 mm in diameter; $3.5 \mu\text{m}$ particle size) at a
191 constant temperature of 25°C . The mobile phase (solvent) and respective
192 gradient followed the method developed by Zapata et al. (2000), discussed and
193 optimized by Mendes et al. (2007), with a flow rate of 1 mL min^{-1} , injection volume

194 of 100 μL and 40 min runs. All the studied pigments were identified from both
195 absorbance spectra and retention times, and the concentrations were calculated
196 from the signals in the photodiode array detector in comparison with commercial
197 standards obtained from DHI (Institute for Water and Environment, Denmark).
198 The peaks were integrated using LC-Solution software, and all peak integrations
199 were checked manually and corrected when necessary. A quality assurance
200 threshold procedure, through application of limit of quantification (LOQ) and limit
201 of detection (LOD), was applied to pigment data to reduce the uncertainty of
202 pigments found in low concentrations (Hooker et al. 2005). The LOQ and LOD
203 procedures were performed according to Mendes et al. (2007). Furthermore, the
204 quality assurance (QA) was performed with the calibration of the HPLC peaks
205 using the pigment standards from DHI (Hooker et al. 2012; Canuti et al. 2022).
206 The quality control (QC), in turn, was performed using a linear relationship
207 between accessory pigments (all carotenoids plus chlorophylls *b* and *c*) and the
208 total chlorophyll *a* (the sum of Chl-*a* and chlorophyllide *a*) to either accept or
209 eliminate specific samples according to Aiken et al. (2009). In order to correct for
210 losses and volume changes, pigment concentrations were normalized to the
211 internal standard (Hooker et al. 2012). It is important to highlight that
212 phytoplankton pigment analysis was performed at the maximum six months after
213 the sampling to each cruise.

214 The absolute (mg m^{-3} Chl-*a*) and relative (%) contribution of phytoplankton
215 chemotaxonomic groups were estimated via CHEMTAX software v1.95 (Mackey
216 et al. 1996). Seven algal groups were chosen for CHEMTAX analysis based on
217 initial pigment ratios derived for the NAP, including the peridinin-lacking
218 dinoflagellates (dinoflagellates type-B, identified by minor concentration pigments

219 such as Chl c_2 -monogalactosyldiacylglycerol ester and gyroxanthin diester;
220 Mendes et al. 2018). The groups resolved include diatoms type-A, diatoms type-
221 B, dinoflagellates type-A, dinoflagellates type-B, cryptophytes, haptophytes type
222 8 (*Phaeocystis antarctica*) and green flagellates. The two types of diatoms and
223 dinoflagellates were grouped as a same chemotaxonomic group: the diatoms
224 (sum of diatoms type-A and diatoms type-B) and the dinoflagellates (sum of
225 dinoflagellates type-A and dinoflagellates type-B), respectively. The mixed
226 flagellates were derived from the sum of *P. antarctica* and green flagellates - two
227 groups with similar distribution and low biomass accumulation.

228 CHEMTAX results were optimized following Wright et al. (2009).
229 Procedure of quality-control was performed by microscopic analysis. There was
230 a significant linear relationship, considering the entire dataset, with p-value <
231 0.001 between cell density (cells L^{-1}) via microscopy analysis and absolute
232 concentration via HPLC/CHEMTAX analysis of diatoms, dinoflagellates, *P.*
233 *antarctica* and cryptophytes with R^2 (n): 0.6 (77), 0.7 (77), 0.6 (66) and 0.8 (75),
234 respectively. There was no correlation for green flagellates, presumably due to
235 their low biomass contributions (usually < 0.2 $mg\ m^{-3}$ Chl-a) and small size cell,
236 difficult to identify by light microscopy. The significant linear relationship (n = 77,
237 R^2 : 0.7 and p < 0.0001) in general correlation considering the total sum of cell
238 density and Chl-a, supported the accuracy of the CHEMTAX initial matrix used
239 here.

240 Three types of Chl-a degradation products: chlorophyllide-a (Chlide-a),
241 pheophytin-a (Phytin-a), and pheophorbide-a (Phide-a) were identified and
242 quantified by HPLC analysis. Phytin-a and Chlide-a are derived from Chl-a by
243 losing the Mg atom and the phytol chain, respectively; while the loss of both Chl-

244 a structures generates the Phide-a (Shuman and Lorenzen 1975). The loss of Mg
245 atom is associated with zooplankton gut-related acid exposure, whereas phytol
246 chain can be removed by light action and/or cell stress (Moreth and Yentsch
247 1970). Phaeopigments have long been observed in the faecal pellets of
248 zooplankton organisms (Coelho et al. 2011). Therefore, we used the sum of the
249 Phytin-a and Phide-a as a proxy of grazing pressure, and Chlide-a as a proxy of
250 senescence of phytoplankton cells. These two indices were divided by the total
251 of degradation products plus Chl-a (sum of Chl-a, Phytin-a, Phide-a and Chlide-
252 a), and represented as a percentage (Costa et al. 2021).

253 Species composition and cell density of phytoplankton community were
254 assessed by microscopic analysis. Settling chambers (2, 10 or 50-mL settling
255 volume) were inspected on an Axiovert 135 ZEISS inverted microscopic
256 (Utermöhl 1958, Sournia 1978) at 100x, 200x and 400x magnification, following
257 the previous literature (e.g., Lund et al. 1958). Species-specific cell biovolumes
258 ($\mu\text{m}^3 \text{L}^{-1}$) were estimated to diatoms by measuring cell dimensions (i.e., length,
259 width and height) and applying respective similar geometric shapes (Hillebrand
260 et al. 1999). Diatom genera *Asteromphalus*, *Chaetoceros*, *Corethron*, *Eucampia*,
261 *Odontella*, *Rhizosolenia*, *Proboscia*, *Stellarima* and *Thalassiosira* were assigned
262 as centric diatoms. Diatom genera *Fragilariopsis*, *Haslea*, *Manguinea*, *Nitzschia*,
263 *Pinnularia*, *Plagiotropis*, *Pseudo-nitzschia* and *Thalassiothrix* along with diatom
264 family Naviculaceae were assigned as pennate diatoms.

265

266 **Krill abundance.** Two distinct datasets of Antarctic krill, *Euphausia superba*
267 (hereafter, 'krill'), were used in this study. Post-larval krill abundance data during

268 the summer (January and February) between 2014–2016 along the mid-southern
269 WAP were obtained from the KRILLBASE (Atkinson et al. 2017). Standardised
270 numerical density (number of individuals m^{-2}) to a single relatively efficient
271 sampling method was used to reduce possible artefacts arising from differences
272 in sampling method in KRILLBASE (Atkinson et al. 2008). Data of post-larval krill
273 abundance during the late winter (August and September) between 2014–2016
274 along the NAP were obtained in Walsh et al. (2020); please see this reference for
275 further details. Sampling grid for both krill datasets is shown in Supplementary
276 Fig. 1. Although our study focus is spring/summer periods, we use winter post-
277 larval krill dataset to support summer krill abundance along the NAP region, as
278 krill stock from the spring/summer tends to be related to that of autumn/winter
279 (Walsh et al. 2020).

280

281 **Remote sensing measurements.** Daily remote sensing reflectance data with
282 spatial resolution of 4x4 km were acquired from the ESA Ocean Colour Climate
283 Change Initiative (OC-CCI; Sathyendranath et al. 2019) product (v5) for the
284 period of 2009–2019. The remote sensing reflectance data were then used to
285 estimate Chl-a through the OC4-SO, a new regional Chl-a algorithm specifically
286 devised to increase the accuracy and reduce the bias of satellite Chl-a
287 measurements in the WAP (Ferreira et al. 2022). Satellite Sea Surface
288 Temperature (SST; °C) and sea ice fraction (%; hereafter sea ice concentration)
289 for the same period were extracted from the ESA SST CCI and C3S global Sea
290 Surface Temperature Reprocessed product (available at CMEMS; Merchant et
291 al. 2019). This product provides gap-free daily-averaged data with a spatial
292 resolution of 5x5 km at a global level. Sea ice duration (days) was defined as an

293 interval between the sea ice advance in autumn and sea ice retreat in spring. Day
294 of advance was identified when sea ice concentration first exceeded 15% (i.e.,
295 the approximate ice edge) for at least five days, whereas the day of retreat was
296 identified when sea ice concentration dropped below 15% after the winter
297 (Stammerjohn et al. 2008).

298 For all measured variables (except sea ice duration), daily means were
299 calculated for each subregion (north and south; Fig. 1) from early November to
300 the end of March (defined as spring/summer here) between 2013/2014,
301 2014/2015 and 2015/2016. Considering an extended temporal gap, the
302 spring/summer decadal average (2009–2019) was also determined to SST, sea
303 ice concentration/duration and Chl-*a* as a baseline to estimate anomalies during
304 the analysed spring/summer periods (Fig. 1). Average autumn/winter to sea ice
305 concentration was defined from early May to late October, being calculated to the
306 decadal average and spring/summer of 2013/2014, 2014/2015 and 2015/2016
307 (Supplementary Table 1).

308

309 **Statistical analysis.** As there were monthly similarities in the analysed
310 parameters between years, we grouped the same months and applied the
311 nonparametric Kruskal-Wallis test (2013/2014 and 2014/2015) to assess
312 differences on parameters over the phytoplankton seasonal succession (see
313 Figs. 3 and 5, and Supplementary Figs. 4 and 5). To investigate distribution
314 patterns during the 2013/2014 and 2014/2015 spring/summer, we compared
315 surface *in situ* temperature, surface *in situ* salinity and MLD associated with the
316 high proportion of the main phytoplankton groups (> 45% to the total Chl-*a*; Fig.

317 4). Furthermore, considering remote sensing measurements, tests of ANOVA
318 and Tukey were applied to determine spring/summer difference (i.e., 2013/2014,
319 2014/2015 and 2015/2016) in parameters (SST, sea ice concentration and Chl-
320 a) between years within each subregion (north and south; Fig. 1). Data were log-
321 transformed to assure a normal distribution and tests of Shapiro and Bartlett were
322 applied prior to ANOVA test. Krill abundance datasets were also tested
323 (Supplementary Fig. 8). However, even log-transformed, they did not show a
324 normal distribution, preventing to apply a parametric test. Krill density can range
325 from zero to vast swarms even in a short spatial scale (Bahlai et al. 2021), as we
326 observed in the datasets analysed here by the standard error (Supplementary
327 Fig. 8). There was a clear difference in average krill abundance between years
328 due to the sampling frequency of high krill density (i.e., high density values in
329 some years were more frequent than in others, generating high and different
330 standard error values between years). However, the datasets with zero-inflated
331 and very low values, such as < 1 individual m^{-2} , precluded any statistical
332 difference, even applying a nonparametric test.

333 To quantify and describe how environmental parameters may be
334 modulating phytoplankton biomass accumulation, we applied generalized linear
335 models (GLMs) with gamma distribution using a log-link function. We used R
336 software for all statistical analyses. Models were constructed to absolute
337 concentrations of phytoplankton groups (i.e., centric diatoms, pennate diatoms,
338 dinoflagellates, cryptophytes and mixed flagellates) as a function of *in situ*
339 environmental parameters: surface temperature, surface salinity, MLD, dissolved
340 inorganic nitrogen (DIN), grazing index and senescence index (Table 1). Biomass
341 estimation of centric and pennate diatoms cannot be separately performed by

342 HPLC/CHEMTAX analysis in terms of mg m^{-3} Chl-*a*, as they do not have specific
343 biomarker pigments (Costa et al. 2022). The significant correlation (R^2 : 0.55, *p*-
344 value < 0.0001 and $n = 60$) between absolute concentrations of diatoms and
345 biovolume measurements (a sum of pennate and centric diatoms) indicates a
346 convergence between both biomass estimations. Therefore, we used biovolume
347 values ($\mu\text{m}^3 \text{ L}^{-1}$) to centric and pennate diatoms to construct their biomass
348 accumulation models, and absolute concentrations (mg m^{-3} Chl-*a*) derived from
349 HPLC/CHEMTAX analysis to the others (i.e., dinoflagellates, cryptophytes and
350 mixed flagellates). It is important to highlight that models were separately
351 constructed to each phytoplankton group. To modulate phytoplankton biomass
352 accumulation, models were constructed to the summer months (i.e., February
353 and March) considering a large number of samples and heterogeneous
354 distribution of phytoplankton groups. Different from the summer months,
355 phytoplankton groups during November did not have a large biomass
356 accumulation (see Fig. 3). The low biomass accumulation precluded to construct
357 models during November months. Model selection associated with the *in situ*
358 environmental parameters that most explained the biomass accumulation of
359 phytoplankton groups was based on the Akaike information criterion (AIC) and
360 pseudo- R^2 values (Table 1).

361 Although macronutrient concentrations (i.e., DIN, phosphate and silicic
362 acid) were not limiting to phytoplankton biomass accumulation during the
363 spring/summer periods studied here, we used DIN to examine the moment by
364 which a given group would be occupying a specific niche. For example,
365 phytoplankton groups with positive correlation regarding to DIN would be
366 occupying the environment in a first stage, while those groups with negative

367 correlation would be occupying in a secondary stage. In this line, it is also
368 plausible that those groups showing negative correlation with DIN could be
369 associated with shallow mixing layers and, consequently, with meltwater input
370 which may cause a nutrient concentration dilution in subsurface ocean. We also
371 applied GMLs with gamma distribution and log-link function to assess positive or
372 negative correlations of the major phytoplankton groups (i.e., centric and pennate
373 diatoms, dinoflagellates and cryptophytes) regarding to each other, using their
374 absolute concentrations. It is expected that phytoplankton groups showing co-
375 existence patterns demonstrate positive correlation to each other, and vice versa
376 (Costa et al. 2021).

377

378 **Results/discussion**

379 Spring/summer (November–March) of 2013/2014 and 2014/2015 in both
380 NAP subregions had a negative sea surface temperature anomaly (SST) relative
381 to the decadal average (2009–2019; Fig. 1a,b). The opposite was observed on
382 sea ice concentration, which showed positive anomalies (Fig. 1c). Average
383 spring/summer sea ice concentration (south and north subregions, respectively)
384 was higher during 2013/2014 (1.1% and 1.7%) and 2014/2015 (0.8% and 1.1%)
385 than the decadal average (0.4% and 0.8%; Supplementary Table 1). This
386 indicates a sea ice persistence during these spring/summer periods to the
387 decadal pattern, which could potentially increase stratification processes. These
388 patterns were similar to those found in the 2015/2016 spring/summer (Fig. 1b,c
389 and Supplementary Table 1). Colder conditions and higher sea ice extent during
390 this period of 2015/2016 associated with an extreme El Niño event were linked to

391 large diatom blooms along the NAP (Costa et al. 2021). However, despite
392 similarities on SST and sea ice concentration, this pattern was not reproduced in
393 both NAP subregions during the spring/summer of 2013/2014 and 2014/2015,
394 which showed negative Chl-*a* anomalies (Fig. 1d).

395 In the south subregion, the periods of 2013/2014 and 2014/2015, similar
396 to 2015/2016, showed positive sea ice duration anomalies (112, 122 and 126
397 days, respectively) relative to the decadal average (101 days). On the contrary,
398 there was little variability on sea ice duration to the decadal pattern in the north
399 subregion (Supplementary Table 1). Average autumn/winter (May–October) sea
400 ice concentration in both NAP subregions (south and north subregions) during
401 2013/2014 (28.4% and 42.8%) and 2015/2016 (27.1% and 37.6%) was higher
402 than the decadal average (20.2% and 32.3%), in contrast to the autumn/winter of
403 2014/2015 (12.7% and 26.9%, respectively). In fact, there was no pattern
404 between sea ice concentration/duration and Chl-*a* (Figs. 1c-d and Supplementary
405 Table 1). For example, in the south subregion, there was no statistical sea ice
406 concentration difference between the spring/summer periods (Fig. 1c and
407 Supplementary Table 1). On the contrary, in the north subregion, sea ice
408 concentration during 2013/2014 and 2014/2015 was different in relation to the
409 2015/2016 spring/summer (Fig. 1c and Supplementary Table 1). Regardless of
410 differences in sea ice dynamics, however, Chl-*a* anomalies in both NAP
411 subregions were substantially higher during the spring/summer of 2015/2016
412 (Fig. 1d).

413 The sea ice retreat-driven melting associated with the increased SST
414 triggered phytoplankton biomass accumulation during the spring/summer (Fig.

415 2). Accordingly, the highest Chl-*a* peak (10.5 and 10.4 mg m⁻³ Chl-*a*, respectively)
416 occurred between December and January along the south subregion during the
417 2013/2014 and 2014/2015 spring/summer (Fig. 2), while during the
418 spring/summer of 2015/2016 there was a delay in the highest Chl-*a* peak (15.2
419 mg m⁻³ Chl-*a* in the south subregion) occurring between January and February
420 (Supplementary Fig. 2). The link between sea ice retreat and increased Chl-*a*
421 values was only observed in the south subregion, having a discrepancy along the
422 north subregion (Fig. 2a,c). Presumably, advection processes may have had a
423 large influence on this discrepancy (Fig. 2b,d), as surface waters from the
424 Gerlache Strait are advected northward along the NAP (i.e., into the Bransfield
425 Strait in the north subregion; Zhou et al. 2002, Damini et al. 2023). Therefore,
426 phytoplankton biomass produced in the south subregion associated with a
427 southward sea ice melting could have been laterally advected northward,
428 explaining the lack of link between sea ice retreat and Chl-*a* accumulation in the
429 north subregion (Fig. 2; Costa et al. 2021). Additionally, the remote sensing
430 measurements of SST converged with our *in situ* temperature dataset (Fig. 3).
431 Surface *in situ* temperature showed a significant increase from the late spring
432 (November) to summer months (February and March), associated with a
433 significant decrease of surface salinity, reduction in MLD and increased Chl-*a*
434 values (Fig. 3).

435 There was a significant difference on physical parameters and Chl-*a*
436 between the late spring and summer months along the NAP (Fig. 3). In general,
437 environmental conditions to phytoplankton community are more stressful during
438 spring, due to intense fluctuations in light exposure (Joy-Warren et al. 2019) and
439 greater instability (i.e., mixing) in water column structure (Fig. 3c). This leads to

440 a high homogeneity in phytoplankton community composition (i.e., no bloom
441 formation) associated with smaller cells in respect to the summer, when large
442 cells prevail (Rozema et al. 2017; Costa et al. 2021). These previous
443 observations partially agree with our results. The microphytoplankton proportion
444 (26%) was in fact lower than nano- and picophytoplankton proportion during the
445 late spring (42% and 32%, respectively; Supplementary Fig. 3). However,
446 opposite to what could be expected (Petrou et al. 2016), microphytoplankton had
447 a significantly lower proportion during the summer months (February and March
448 – 10% and 4%), in contrast to the nano- (54% and 55%) and picophytoplankton
449 (36% and 41%, respectively; Supplementary Fig. 3). The macronutrient
450 concentrations were highly abundant during the late spring and summer months
451 ($> 14 \mu\text{M}$, $> 0.3 \mu\text{M}$ and $> 20 \mu\text{M}$ of DIN, phosphate and silicic acid, respectively;
452 data not shown) and, although micronutrient measurements were not performed
453 here, dissolved iron is also available in high concentrations ($> 1 \text{ nM}$) along the
454 WAP coastal waters (Annett et al. 2017; Pan et al. 2020). Therefore, these results
455 indicate that such unexpected pattern associated with the microphytoplankton
456 cells was likely linked with physical-biological drivers.

457 In the southern WAP sector, a conceptual model was developed to predict
458 phytoplankton community composition based on previous winter sea ice duration
459 (Rozema et al. 2017). Low biomass summers coupled to low previous winter sea
460 ice have been characterized for a persistence of smaller phytoplankton cells (i.e.,
461 small diatoms and nanoflagellates) from the spring, while the high biomass
462 summers/high winter sea ice years had a strong contribution of large diatoms
463 (Rozema et al. 2017). Although there was no relationship found here between
464 sea ice duration and phytoplankton biomass during the summer (Fig. 1 and

465 Supplementary Table 1), the conceptual model shows similarities with our
466 phytoplankton size fractionation measurements (Supplementary Fig. 3). The
467 results suggest that both spring/summer of 2013/2014 and 2014/2015 had a
468 phytoplankton community composition associated with low biomass
469 accumulation (Fig. 1), characterized by persistent smaller cells during the
470 summer (Supplementary Fig. 3). Moreover, converging with our *in situ* sampling,
471 the negative Chl-*a* anomalies from remote sensing measurements further support
472 the low phytoplankton biomass accumulation during our study periods (Fig. 1d).

473 Diatoms, cryptophytes and dinoflagellates showed a clear contribution
474 (median of 40%, 20% and 20%, respectively) during the spring, with a
475 background presence of mixed flagellates (median of 15%; Supplementary Figs.
476 4 and 5). However, not prevailing as expected during the summer, diatoms
477 showed a low biomass proportion during February months (2014 and 2015),
478 equivalent or lower than the proportion of cryptophytes and dinoflagellates
479 (Supplementary Figs. 4 and 5). The absolute concentration of diatoms in
480 February was similar to that measured in November, significantly increasing in
481 March, but no forming bloom (Supplementary Fig. 4b). Dinoflagellates and mixed
482 flagellates showed an increase in absolute terms in both February and March,
483 while cryptophytes showed higher concentrations in February (Supplementary
484 Figs. 4d and 5b,d).

485 During the late spring (left side regarding the vertical dashed red line in
486 Fig. 4a), cryptophytes dominated under relatively lower salinity values (<34)
487 compared with centric diatoms (>34; Fig. 4a). This indicates that cryptophytes
488 (*Geminigera*; Supplementary Table 2) could be preferentially accumulating

489 biomass closer to the sea ice edge, contrary to the centric diatoms. Presumably,
490 there was a higher stabilization surrounding the sea ice boundary, generating
491 shallower mixing layers which are favourable to cryptophyte development
492 (Mendes et al. 2018, 2023). The most common genera of centric diatoms during
493 November were *Chaetoceros*, *Corethron* and *Thalassiosira* (Supplementary
494 Table 2). Less evident in this onset stage of growth, pennate diatoms (mainly
495 composed by *Fragilariopsis*) only showed high proportion in an occasional station
496 (Fig. 4a). Dinoflagellates (mainly composed by *Gymnodinium*) and mixed
497 flagellates (mainly composed by *Phaeocystis antarctica* and Prasinophyceae) did
498 not show high proportions during the late spring (Fig. 4 and Supplementary Table
499 2).

500 Different from the late spring, during the summer (right side regarding the
501 vertical dashed red line in Fig. 4a), there was a marked increase in high
502 proportion of pennate diatoms and dinoflagellates, while centric diatoms were
503 less evident (Fig. 4a), which converges with the decreased microphytoplankton
504 proportion (Supplementary Fig. 3). This increase of pennate diatoms was
505 associated with a higher abundance of *Fragilariopsis*, *Pseudo-nitzschia* and
506 Naviculaceae (Supplementary Table 2). *Gymnodinium* was also the most
507 abundant dinoflagellate genus during the summer, while *Thalassiosira* showed
508 the highest contribution to centric diatoms (Supplementary Table 2). The
509 phytoplankton taxa were not observed in a specific range of temperature, except
510 for dinoflagellates that dominated in warmer conditions (in general $>1^{\circ}\text{C}$; Fig. 4a).
511 On the contrary, under salinity influence, pennate diatoms and cryptophytes were
512 preferentially distributed in lower salinity (<34) than the centric diatoms and
513 dinoflagellates (>34). This reflects on MLD distribution range of these groups (Fig.

514 4b). Pennate diatoms and cryptophytes were distributed in shallower MLDs
515 (preferentially <25m) compared with the centric diatoms and dinoflagellates
516 (preferentially >25m).

517 There were no significant differences on physical parameters between
518 November 2013 and 2014 in relation to November 2015 (Supplementary Fig. 6),
519 suggesting similar conditions between these periods to phytoplankton community
520 composition at the initial stage of growth. On the other hand, although surface *in*
521 *situ* temperature showed similarities, there was a significant difference on surface
522 salinity and MLD values in February 2014 and 2015 compared with February
523 2016. Surface salinity was significantly lower in February 2014 and 2015, which
524 reflected in shallower MLDs, compared with February 2016 (Supplementary Fig.
525 7). These differences in physical parameters influenced on biological
526 compartments, while there was a biomass accumulation of centric diatoms of up
527 to $594 \times 10^6 \mu\text{m}^3 \text{L}^{-1}$ between February 2014 and 2015, during February 2016
528 centric diatom biomass accumulation reached $33,922 \times 10^6 \mu\text{m}^3 \text{L}^{-1}$ associated
529 with the *Odontella weissflogii* bloom (Costa et al. 2020). Therefore, these results
530 link lower centric diatom biomass accumulation to shallower MLDs and lower
531 salinity values during February 2014 and 2015 along the NAP.

532 Glacier retreat is another important source of meltwater input along the
533 NAP (Pan et al. 2020). Its influence in water column stratification is apparently
534 different regarding to sea ice melting (Rozema et al. 2017). While winter sea ice
535 amount has been associated with water column stratification magnitude over the
536 phytoplankton seasonal succession, glacier meltwater has been associated with
537 localized stratification processes, modulating phytoplankton community

538 composition along the NAP summer (Mendes et al. 2013, 2018; Rozema et al.
539 2017; Costa et al. 2021). Indeed, high cryptophyte proportion has been found in
540 shallower MLDs (<20m) coupled with localized glacier meltwater input (Mendes
541 et al. 2023), while diatoms, especially their centric shapes, have been observed
542 to preferentially accumulate biomass in deeper MLDs (>20m; Costa et al. 2021).
543 In addition, pennate diatoms have also been associated with seawater of low
544 salinity (<34; Mascioni et al. 2021). Experiments have proposed shifts from
545 centric to pennate forms under low salinity treatment due to the physiological
546 stress (Hernando et al. 2015). However, we do not have evidence for such stress.
547 The salinity values observed here (>33) were much higher than the low salinity
548 treatment (30) tested by Hernando et al. (2015). On the other hand, there was a
549 significant relationship between surface salinity and MLD, characterizing a
550 preferential distribution range to phytoplankton groups in water column (Fig. 4b).

551 Phytoplankton along the NAP coastal ecosystems has a bottom-up control
552 associated with water column structure-driven light availability (Saba et al. 2014),
553 due to high concentrations of micro- (e.g., dissolved iron) and macro-nutrients
554 (e.g., silica, phosphate and nitrate) in the upper ocean layers (Annett et al. 2017;
555 Pan et al. 2020). Therefore, markedly shallow MLDs could likely be modulating
556 the phytoplankton development along the NAP and, consequently, biomass
557 accumulation by inducing excess light conditions in confined layers (Petrou et al.
558 2016; Mendes et al. 2023). However, such potential photophysical stress
559 associated with meltwater input would have an influence on relatively short period
560 of time regarding to the whole seasonal succession. That is, the light condition in
561 shallower MLDs could explain differences on Chl-*a* values between February
562 months, but not for the entire phytoplankton seasonal succession (Fig. 1d). The

563 sea ice concentration-driven stratification process during the spring/summer
564 should be similar between the seasonal periods of 2013–2016 (Fig. 1c and
565 Supplementary Table 1), thus expecting higher Chl-a values during the
566 2013/2014 and 2014/2015 spring/summer (Saba et al. 2014; Rozema et al.
567 2017). Therefore, this indicates that the low Chl-a values in these spring/summer
568 periods were also driven by another critical factor.

569 The observed pattern of centric diatoms was unexpected during the
570 spring/summer of 2013/2014 and 2014/2015 (Fig. 5). It would be expected that
571 centric diatoms had biomass increase to summer months, forming bloom events
572 (Petrou et al. 2016). However, their biomass contributions (in terms of biovolume
573 values) showed a significant decrease from the late spring to summer months
574 (Fig. 5a). This unexpected pattern was coupled with a significant contribution
575 increase of pennate diatoms (Fig. 5b), contrasting with the 2015/2016
576 spring/summer when there was a marked contribution of centric diatoms,
577 especially during the *Odontella weissflogii* bloom (Costa et al. 2020, 2021).
578 Likewise, there was also a significant increase on grazing and senescence
579 indices from the late spring to summer months (Fig. 5c,d). We presume Chl-a
580 that was not ingested during grazing activity (related to “sloppy feeding” process),
581 and thus dispersed in seawater, could easily lose the phytol chain by light action
582 (Moreth and Yentsch 1970). This could be explaining the concomitant increase
583 on grazing and senescence indices over the spring/summer (Fig. 5c,d). These
584 results suggest that shifts from centric to pennate diatoms associated with a
585 selective grazing pressure may be occurring during the phytoplankton seasonal
586 succession along the NAP.

587 Another independent evidence of the top-down control importance during
588 these analysed succession periods was found in Antarctic krill abundance
589 (Supplementary Fig. 8). There was a higher average krill density during the
590 summer (mean \pm standard error; 35 ± 22 and 62 ± 30 individuals m^{-2}) and
591 following winter (1570 ± 595 and 1121 ± 516 individuals m^{-2} , respectively) of 2014
592 and 2015 compared with the summer (18 ± 7 individuals m^{-2}) and winter ($505 \pm$
593 135 individuals m^{-2}) of 2016 (Supplementary Fig. 8). These results suggest a
594 hypothetical scenario where krill stocks were potentially higher during the
595 seasonal periods of 2013/2014 and 2014/2015 off the NAP, which could be
596 reflecting in an increased grazing pressure on phytoplankton community.
597 Although the top-down control on phytoplankton can also be exerted by other
598 zooplankton species, such as copepods and salps, krill is the major
599 macrozooplankton grazer near the coast and over the shelf along the WAP,
600 efficiently grazing on large centric diatoms ($>20 \mu m$), which are responsible by
601 bloom formation (Haberman et al. 2003; Henley et al. 2019; Costa et al. 2020).
602 In fact, along the NAP, low (high) *in situ* Chl-*a* during February was associated
603 with negative (positive) satellite Chl-*a* anomalies during the spring/summer of
604 2013/2014 and 2014/2015 (2015/2016) (Fig. 1 and Supplementary Fig. 8c). This
605 link between Chl-*a* and krill abundance also converges with previous findings,
606 which have found evidence for a relationship between interannual variability of
607 phytoplankton biomass and krill reproduction (Garibotti et al. 2005; Saba et al.
608 2014).

609 Modelling absolute biomass of centric diatoms (in terms of biovolume; μm^3
610 L^{-1}) as a function of environmental parameters demonstrates that there was a
611 significant positive correlation between their biomass and MLD and DIN (Table 1

612 and Supplementary Fig. 9). These results agree with the preferential distribution
613 of centric diatoms in relatively deeper MLDs (Costa et al. 2021), indicating an
614 initial environment occupation due to the positive correlation with DIN (see
615 Methods). Similarly to the centric diatoms, suggesting a coexistence pattern,
616 absolute biomass (mg m^{-3} Chl-*a*) of dinoflagellates showed a significant positive
617 correlation with MLD and DIN (Table 1 and Supplementary Fig. 9). The positive
618 correlation between absolute biomass of centric diatoms and dinoflagellates
619 further indicates that both phytoplankton groups may be co-occurring
620 (Supplementary Fig. 10a and Table 3). This coexistence pattern has already been
621 observed along the NAP, with dinoflagellates predominantly occupying the
622 environment as large centric diatoms had left the system (Costa et al. 2021).
623 Furthermore, temperature did not explain biomass accumulation of
624 dinoflagellates as a whole, which suggests that their higher proportion in warmer
625 conditions was an exceptional biomass accumulation event (see Fig. 4), mainly
626 associated with *Gymnodinium* spp. (Supplementary Table 2). In fact,
627 *Gymnodinium* spp. also had high abundance values during the late spring,
628 supporting that colder temperatures were not limiting their development
629 (Supplementary Table 2). Therefore, MLD seems to be the key physical driver of
630 this emerging group along the NAP coastal waters, although the link between
631 dinoflagellates and warmer temperatures should be further understood,
632 especially considering interspecific differences (Costa et al. 2021).

633 Biomass of pennate diatoms (in terms of $\mu\text{m}^3 \text{L}^{-1}$) and cryptophytes (mg
634 m^{-3} Chl-*a*) was also modelled as a function of environmental parameters (Table
635 1). They demonstrated a significant negative correlation with DIN (Table 1 and
636 Supplementary Fig. 9), indicating that both groups could be occupying the

637 environment in a secondary stage or associated with subsurface ocean dilution
638 from the meltwater input (see Methods). However, despite distribution similarities,
639 there was no evidence for coexistence between pennate diatoms and
640 cryptophytes, as their absolute biomass had no significant correlation
641 (Supplementary Fig. 10b and Table 3). Furthermore, cryptophytes (pennate
642 diatoms) showed a significant negative (positive) correlation with temperature
643 and grazing index (Table 1). These opposite results suggest, given the biomass
644 accumulation of both groups in shallower MLDs (Fig. 4), that cryptophytes could
645 be occupying the environment just after the glacier meltwater input, which
646 generates colder subsurface temperatures, becoming warmer afterwards due to
647 increasingly retention of incident solar radiation (Lima et al. 2022). Indeed,
648 negative correlation between cryptophytes and grazing index supports this
649 interpretation (i.e., higher cryptophyte biomass correlated with lower grazing
650 index values), as recent meltwater input due to its dilution could mitigate grazing
651 pressure in lower salinity and stratified waters (Mendes et al. 2023).

652 Absolute biomass of major phytoplankton groups was also modelled as a
653 function of each other to assess potential coexistence pattern (see Methods). As
654 a result, there were negative correlations between absolute concentration of
655 cryptophytes in relation to centric diatoms and dinoflagellates, indicating a clear
656 niche segregation between these groups (Supplementary Table 3 and
657 Supplementary Fig. 10c-f). On the other hand, there were no correlations in
658 models of centric diatoms, dinoflagellates and cryptophytes modelled as a
659 function of pennate diatoms (Supplementary Table 3 and Supplementary Fig.
660 10c-f). These results further support that cryptophytes could be occupying a free
661 environment in confined layers just after glacier meltwater input, and pennate

662 diatoms would be occupying the environment in a transition process of MLD
663 deepening, in which under favorable conditions large centric diatoms prevail (Fig.
664 4 and Table 1). Moreover, positive significant correlation between absolute
665 biomass (mg m^{-3} Chl-*a*) of mixed flagellates and MLD denotes that these small
666 cells increased their biomass in deeper mixing layers (Table 1 and
667 Supplementary Fig. 9). Probably, these small nanoflagellates had a standard
668 stock, characterized by a background presence on phytoplankton community
669 composition, predominantly occupying the environment after large centric
670 diatoms and dinoflagellates had left the system in a final stage of seasonal
671 succession (Pan et al. 2020). This pattern is supported by the positive correlation
672 between mixed flagellates and senescence index (i.e., higher mixed flagellate
673 biomass correlated with higher senescence index values; Table 1 and
674 Supplementary Fig. 9).

675 The lack of MLD statistical significance in models of pennate diatoms and
676 cryptophytes indicates that although both groups preferentially accumulated
677 biomass in shallower MLDs, they did not exclusively occur under such conditions,
678 in contrast to the patterns of centric diatoms and dinoflagellates (Table 1 and
679 Supplementary Fig. 9). These results suggest that pennate diatoms and
680 cryptophytes opportunistically accumulated biomass in the absence of centric
681 diatoms, the common dominant phytoplankton group in Antarctic waters (Malviya
682 et al. 2016; Petrou et al. 2016; Costa et al. 2022). High flexibility of pennate
683 diatoms and cryptophytes to cope with potential excess light in confined layers
684 could be favouring their prevalence in shallower MLDs (Petrou et al. 2016;
685 Mendes et al. 2023). Furthermore, sinking process of large centric diatoms out of
686 the upper layers under highly stratified conditions cannot be disregarded (Costa

687 et al. 2021). We also found evidence for top-down control over the phytoplankton
688 seasonal succession, potentially driving biomass accumulation and species
689 composition (Fig. 5 and Supplementary Fig. 8). Indeed, the significant positive
690 correlation between pennate diatoms and grazing index, contrasted by the
691 significant negative correlation between centric diatoms and senescence index
692 (Table 1 and Supplementary Fig. 9), supports the observed shift between them
693 associated with grazing pressure over the phytoplankton seasonal succession
694 (Fig. 5). These results may explain the decoupling between sea ice
695 concentration/duration and Chl-*a* during the spring/summer of 2013/2014 and
696 2014/2015 along the NAP. Moreover, the delay in the highest Chl-*a* peak
697 occurring between January and February during the spring/summer of 2015/2016
698 may have contributed to potential trophic mismatch between phytoplankton and
699 zooplankton communities (Supplementary Fig. 2). This trophic mismatch could
700 have favoured the bloom formation of large centric diatoms throughout the NAP
701 during 2015/2016 (Costa et al. 2020, 2021), contrasting the spring/summer of
702 2013/2014 and 2014/2015.

703

704 **Final remarks**

705 In short, during the 2013/2014 and 2014/2015 spring/summer, sea ice
706 melting triggered phytoplankton development in the spring (Fig. 2). The Chl-*a*
707 peak occurred between December and January along the south subregion as
708 water column was stratified and shallower MLDs formed (Figs. 2 and 3),
709 decreasing biomass accumulation toward April (Fig. 2). At the initial stage of
710 growth, regardless of biomass accumulation during the summer, phytoplankton

711 community was composed by equivalent proportion and abundance of smaller
712 nanoflagellate cells (i.e., cryptophytes, dinoflagellates, *P. antarctica* and green
713 flagellates) and centric and pennate diatoms (Supplementary Figs. 3-4 and Table
714 2). In general, there was a high homogeneity (i.e., there was not a clear
715 dominance of a given group or bloom formation) in phytoplankton community
716 composition during the late spring, with occasional high proportion of centric
717 diatoms and cryptophytes, closer to the sea ice edge (Figs. 4 and 6). During the
718 summer, on the contrary, phytoplankton community composition varied based on
719 diatom biomass accumulation: high or low biomass conditions. The high biomass
720 condition, characterized by diatom bloom formation, was completely dominated
721 by centric diatoms (i.e., conditions found in the spring/summer of 2015/2016),
722 while the low biomass condition showed a higher proportion of cryptophytes,
723 dinoflagellates and/or pennate diatoms, with a background presence of mixed
724 flagellates (i.e., conditions found in the spring/summer of 2013/2014 and
725 2014/2016; Fig. 6).

726 Moreover, going into the autumn (April onwards), decreased SST and Chl-
727 a (Fig. 2) may be indicating a deepening of MLD due to the increased wind speed,
728 expected after the summer months (Schofield et al. 2018). At this final stage of
729 seasonal succession, phytoplankton community composition in increasingly
730 mixing water columns tends to be dominated by smaller diatoms and
731 nanoflagellate cells, as sea ice begins to advance (Pan et al. 2020).
732 Phytoplankton taxa need to cope with environmental adversity, thriving under
733 severe weather conditions during autumn and winter to start their growing season
734 again, when sea ice comes back to retreat in the next austral spring onwards
735 (Fig. 2; Petrou et al. 2016). Here, patterns of phytoplankton seasonal succession

736 were observed off the NAP, a warming-impacted region in the Southern Ocean,
737 which undergoes critical physical and biological changes in its marine
738 ecosystems (Ducklow et al. 2013). In general, bottom-up control showed a crucial
739 role on development and establishment of phytoplankton groups, despite the
740 short-term decoupling between sea ice concentration/duration and Chl-*a*,
741 associated with the top-down control influence on both phytoplankton biomass
742 accumulation and species composition.

743

744 **References**

745 Aiken, J., Pradhan, Y., Barlow, R., Lavender, S., Poulton, A., Holligan, P.,
746 Hardman-Mountford, N. (2009) Phytoplankton pigments and functional types in
747 the Atlantic Ocean: A decadal assessment, 1995 – 2005. *Deep-Sea Res. Part II*
748 *Top. Stud. Oceanogr.*, 56, 899–917.

749

750 Annett, A.L., Fitzsimmons, J.N., Séguret, M.J., Lagerström, M., Meredith, M.P.,
751 Schofield, O. & Sherrell, R.M. (2017) Controls on dissolved and particulate iron
752 distributions in surface waters of the Western Antarctic Peninsula shelf. *Mar.*
753 *Chem.*, 196, 81–97.

754

755 Aminot, A. & Chaussepied, M. (1983) Manuel des analyses chimiques en milieu
756 marin. Brest, France: Centre National pour L'Exploitation des Océans (CNEXO).

757

758 Atkinson, A., Siegel, V., Pakhomov, E.A., Rothery, P., Loeb, V., Ross, R.M. et al.
759 (2008) Oceanic circumpolar habitats of Antarctic krill. *Mar. Ecol. Prog. Ser.*, 362,
760 1–23.

761

762 Atkinson, A., Hill, S.L., Pakhomov, E., Siegel, V., Anadon, R., Chiba, S. et al.
763 (2017) KRILLBASE: a circumpolar database of Antarctic krill and salp numerical
764 densities, 1926–2016. *Earth Syst. Sci. Data*, 9, 1–18.

765

766 Bahlai, C.A., Hart, C., Kavanaugh, M.T., White, J.D., Ruess, R.W., Brinkman,
767 R.J. (2021) Cascading effects: insights from the U.S. Long Term Ecological
768 Research Network. *Ecosphere*, 12, e03430.

769

770 de Boyer Montégut, C., Madec, G., Fischer, A.S., Lazar, A. & Iudicone, D. (2004)
771 Mixed layer depth over the global ocean: An examination of profile data and a
772 profile based climatology. *J. Geophys. Res.*, 109, C12003.

773

774 Canuti, E., Artuso, F., Bracher, A., Brotas, V., Devred, E., Dimier, C., Giardina, I.,
775 Mendes, C.R., Murawski, S., Peeken, I., Tracana, A., Ras, J. & Wiegmann, S.
776 (2022) The Fifth HPLC Intercomparison on Phytoplankton Pigments (HIP-5)
777 Technical Report. Publications Office of the European Union, Luxembourg,
778 JRC130280.

779

780 Coelho, H., Cartaxana, P., Brotas, V., Queiroga, H. & Serôdio, J. (2011)
781 Pheophorbide *a* in *Hydrobia ulvae* faecal pellets as a measure of
782 microphytobenthos ingestion: variation over season and period of day. *Aquat.*
783 *Biol.*, 13, 119–126.

784

785 Cook, A.J., Holland, P.R., Meredith, M.P., Murray, T., Luckman, A. & Vaughan,
786 D.G. (2016) Ocean forcing of glacier retreat in the western Antarctic Peninsula.
787 *Science*, 353, 283–286.

788

789 Costa, R.R., Mendes, C.R.B., Tavano, V.M., Dotto, T.S., Kerr, R., Monteiro, T.
790 et al. (2020) Dynamics of an intense diatom bloom in the Northern Antarctic
791 Peninsula, February 2016. *Limnol. Oceanogr.*, 65, 2056–2075.

792

793 Costa, R.R., Mendes, C.R.B., Ferreira, A., Tavano, V.M., Dotto, T.S. & Secchi,
794 E.R. (2021) Large diatom bloom off the Antarctic Peninsula during cool conditions
795 associated with the 2015/2016 El Niño. *Commun. Earth. Environ.*, 2, 252.

796

797 Costa, R.R., Mendes, C.R.B., Souza, M.S., Tavano, V.M. & Secchi, E.R. (2022)
798 Chemotaxonomic characterization of the key genera of diatoms in the Northern
799 Antarctic Peninsula. *An. Acad. Bras. Cienc.*, 94, e20210584.

800

801 Damini, B.Y., Costa, R.R., Dotto, T.S., Mendes, C.R.B., Torres-Lasso, J.C.,
802 Azaneu, M.V.C, Mata, M.M. & Kerr, R. (2023). Antarctica Slope Front bifurcation
803 eddy: A stationary feature influencing CO₂ dynamics in the northern Antarctic
804 Peninsula. *Prog. Oceanogr.*, 212, 102985.

805

806 Ducklow, H.W., Fraser, W.R., Meredith, M.P., Stammerjohn, S.E., Doney, S.C.,
807 Martinson, D.G. et al. (2013) West Antarctic Peninsula: An ice-dependent coastal
808 marine ecosystem in transition. *Oceanography*, 26, 190–203.

809

810 Ferreira, A., Costa, R.R., Dotto, T.S., Kerr, R., Tavano, V.M., Brito, A.C. et al.
811 (2020) Changes in Phytoplankton Communities Along the Northern Antarctic
812 Peninsula: Causes, Impacts and Research Priorities. *Front. Mar. Sci.*, 7, 576254.

813

814 Ferreira, A., Brito, A.C., Mendes, C.R.B., Brotas, V., Costa, R.R., Guerreiro, C.V.
815 et al. (2022) OC4-SO: A New Chlorophyll-a Algorithm for the Western Antarctic
816 Peninsula Using Multi-Sensor Satellite Data. *Remote Sens.*, 14, 1052.

817

818 Garibotti, I. A., Vernet, M., Smith, R. C. & Ferrario, M. E. (2005) Interannual
819 variability in the distribution of the phytoplankton standing stock across the
820 seasonal sea-ice zone west of the Antarctic Peninsula. *J. Plankton Res.*, 27, 825–
821 843.

822

823 Haberman, K. L., Ross, R.M. & Quetin, L.B. (2003) Diet of the Antarctic krill
824 (*Euphausia superba* Dana): II selective grazing in mixed phytoplankton
825 assemblages. *J. Exp. Mar. Biol. Ecol.*, 283, 97–113.

826

827 Henley, S.F., Schofield, O.M., Hendry, K.R., Schloss, I.R., Steinberg, D.K.,
828 Moffat, C. et al. (2019) Variability and change in the west Antarctic Peninsula
829 marine system: research priorities and opportunities. *Prog. Oceanogr.*, 173, 208–
830 237.

831

832 Hernando, M., Schloss, I.R., Malanga, G., Almandoz, G.O., Ferreyra, G.A.,
833 Aguiar, M.B & Puntarulo, S. (2015) Effects of salinity changes on coastal Antarctic
834 phytoplankton physiology and assemblage composition. *J. Exp. Mar. Biol. Ecol.*,
835 466, 110–119.

836

837 Hillebrand, H., Dürselen, C.D., Kirschtel, D., Pollinger, U. & Zohary, T. (1999)
838 Biovolume calculation for pelagic and benthic microalgae. *J. Phycol.*, 35, 403–
839 424.

840

841 Hooker, S.B. et al. (2005) The second sea-WiFS HPLC analysis round-robin
842 experiment (SeaHARRE-2). NASA Tech. Memo. 2005–212785. Greenbelt, MD:
843 NASA Goddard Space Flight Center.

844

845 Hooker, S.B. et al. (2012) The Fifth SeaWiFS HPLC Analysis Round-Robin
846 Experiment (SeaHARRE-5). NASA Tech. Memo. 2012–217503. Greenbelt, MD:
847 NASA Goddard Space Flight Center.

848

849 Joy-Warren, H.L., van Dijken, L.G., Alderkamp, A.C., Leventer, A., Lewis, K.M.,
850 Selz, V. et al. (2019) Light is the primary driver of early season phytoplankton
851 production along the Western Antarctic Peninsula. *J. Geophys. Res. Oceans*,
852 124, 7375–7399.

853

854 Lima, L.S., Pezzi, L.P., Mata, M.M., Santini, M.F., Carvalho, J.T., Sutil, U.A. et al.
855 (2022) Glacial meltwater input to the ocean around the Antarctic Peninsula:
856 forcings and consequences. *An. Acad. Bras. Cienc.*, 94, e20210811.

857

858 Lund, J.W.G., Kipling, C. & Le Cren, E.D. (1958) The inverted microscope method
859 of estimating algal numbers and the statistical basis of estimations by counting.
860 *Hydrobiologia*, 11, 143-170.

861

862 Mascioni, M., Almandoz, G.O., Ekern, L., Pan, J. & Vernet, M. (2021)
863 Microplanktonic diatom assemblages dominated the primary production but not
864 the biomass in an Antarctic fjord. *J. Marine Syst.*, 224, 103624.

865

866 Mendes, C. R., Cartaxana, P. & Brotas, V. (2007) HPLC determination of
867 phytoplankton and microphytobenthos pigments: Comparing resolution and
868 sensitivity of a C18 and a C8 method. *Limnol. Oceanogr. Methods*, 5, 363–370.

869

870 Mendes, C. R. B., Tavano, V. M., Leal, M. C., Souza, M. S., Brotas, V. & Garcia,
871 C. A. E. (2013) Shifts in the dominance between diatoms and cryptophytes during
872 three late summers in the Bransfield Strait (Antarctic Peninsula). *Polar Biol.*, 36,
873 537–547.

874

875 Mendes, C.R.B., Tavano, V.M., Kerr, R., Dotto, T.S., Maximiano, T. & Secchi,
876 E.R. (2018) Impact of sea ice on the structure of phytoplankton communities in
877 the northern Antarctic Peninsula. *Deep-Sea Res. Part II Top. Stud. Oceanogr.*,
878 149, 111–123.

879

880 Mendes, C.R.B., Costa, R.R., Ferreira, A., Jesus, B., Tavano, V.M., Dotto, T.S.
881 et al. (2023) Cryptophytes: An emerging algal group in the rapidly changing
882 Antarctic Peninsula marine environments. *Glob. Chang. Biol.*, 00, 1–18.

883

884 Merchant, C.J., Embury, O., Bulgin, C.E., Block, T., Corlett, G.K., Fiedler, E. et
885 al. (2019) Satellite-based time-series of sea-surface temperature since 1981 for
886 climate applications. *Sci. Data*, 6, 223.

887

888 Moreth, C.M. & Yentsch, C.S. (1970) The role of chlorophyllase and light in the
889 decomposition of chlorophyll from marine phytoplankton. *J. Exp. Mar. Biol. Ecol.*,
890 4, 238-249.

891

892 Montes-Hugo, M., Doney, S. C., Duclow, H. W., Fraser, W., Martinson, D.,
893 Stammerjohn, S. E. & Schofield, O. (2009) Recent changes in phytoplankton
894 communities associated with rapid regional climate change along the Western
895 Antarctic Peninsula. *Science*, 323, 1470–1473.

896

897 Pan, B.J., Vernet, M., Manck, L., Forsch, K., Ekern, L., Mascioni, M. et al. (2020)
898 Environmental drivers of phytoplankton taxonomic composition in an Antarctic
899 fjord. *Prog. Oceanogr.*, 183, 102295.

900

901 Petrou, K., Kranz, S. A., Trimborn, S., Hassler, C. S., Ameijeiras, S. B., Sackett,
902 O., Ralph, P. J. & Davidson, A. T. (2016) Southern Ocean phytoplankton
903 physiology in a changing climate. *J. Plant Physiol.*, 203, 135–150.

904

905 Rodriguez, F., Varela, M. & Zapata, M. (2002) Phytoplankton assemblages in the
906 Gerlache and Bransfield Straits (Antarctic Peninsula) determined by light
907 microscopy and CHEMTAX analysis of HPLC pigment data. *Deep-Sea Res. Part*
908 *II Top. Stud. Oceanogr.*, 49, 723–747.

909

910 Rozema, P. D., Venables, H.J., van de Poll, W.H., Clarke, A., Meredith, M.P. &
911 Buma, A. G. J. (2017) Interannual variability in phytoplankton biomass and
912 species composition in northern Marguerite Bay (West Antarctic Peninsula) is
913 governed by both winter sea ice cover and summer stratification. *Limnol.*
914 *Oceanogr.*, 62, 235–252.

915

916 Saba, G.K., Fraser, W.R., Saba, V.S., Iannuzzi, R.A., Coleman, K.E., Doney, S.C.
917 et al. (2014) Winter and spring controls on the summer food web of the coastal
918 West Antarctic Peninsula. *Nat. Commun.*, 5, 4318.

919

920 Santos-Andrade, M., Kerr, R., Orselli, I.B.M., Monteiro, T, Matta, M.M. & Goyet,
921 C. (2023) Drivers of Marine CO₂-Carbonate Chemistry in the Northern Antarctic
922 Peninsula. *Glob. Biogeochem. Cycles*, 37, e2022GB007518.

923

924 Sathyendranath, S., Brewin, R.J.W., Brockmann, C., Brotas, V., Calton, B.,
925 Chuprin, A. et al. (2019) An ocean-colour time series for use in climate studies:

- 926 the experience of the ocean-colour climate change initiative (OC-CCI). *Sensors*,
927 19, 4285.
- 928
- 929 Schofield, O., Saba, G., Coleman, K., Carvalho, F., Couto, N. & Ducklow, H. et
930 al. (2017) Decadal variability in coastal phytoplankton community composition in
931 a changing West Antarctic Peninsula. *Deep-Sea Res. Part I Oceanogr. Res.*
932 *Pap.*, 124, 42–54.
- 933
- 934 Schofield, O., Brown, M., Kohut, J., Nardelli, S., Saba, G., Waite, N. & Ducklow,
935 H. (2018) Changes in the upper ocean mixed layer and phytoplankton productivity
936 along the West Antarctic Peninsula. *Phil. Trans. R. Soc. A*, 376, 20170173.
- 937
- 938 Shaman, F.R. & Lorenzen, C.J. (1975) Quantitative degradation of chlorophyll by
939 a marine herbivore. *Limnol. Oceanogr.*, 20, 580-586.
- 940
- 941 Sournia, A. (1978) Phytoplankton manual. Paris: Muse'um National d'Histoire
942 Naturelle, UNESCO.
- 943
- 944 Stammerjohn, S. E., Martinson, D. G., Smith, R. C., Yuan, X. & Rind, D. (2008)
945 Trends in Antarctic annual sea ice retreat and advance and their relation to El
946 Niño–Southern oscillation and Southern Annular Mode variability. *J. Geophys.*
947 *Res. Oceans*, 113, C03S90.
- 948
- 949 Utermöhl, H. (1958) Zur Vervollkommnung der quantitativen phytoplankton
950 Methodik. *Mitt. Int. Ver. Theor. Angew. Limnol.*, 9, 1–38.
- 951
- 952 Varela, M., Fernandez, E. & Serret, P. (2002) Size-fractionated phytoplankton
953 biomass and primary production in the Gerlache and south Bransfield Straits
954 (Antarctic Peninsula) in Austral summer 1995–1996. *Deep-Sea Res. Part II Top.*
955 *Stud. Oceanogr.*, 49, 749–768.
- 956
- 957 Walsh, J., Reiss, C.S. & Watters, G.M. (2020) Flexibility in Antarctic krill
958 *Euphausia superba* decouples diet and recruitment from overwinter sea-ice
959 conditions in the northern Antarctic Peninsula. *Mar. Ecol. Prog. Ser.*, 642, 1–19.
- 960
- 961 Wright, S.W., Ishikawa, A., Marchant, H.J., Davidson, A.T., van den Enden, R.L.
962 & Nash, G.V. (2009) Composition and significance of picophytoplankton in
963 Antarctic waters. *Polar Biol.*, 32, 797–808.

964

965 Zapata, M., Rodríguez, F. & Garrido, J.L. (2000) Separation of chlorophylls and
966 carotenoids from marine phytoplankton: A new HPLC method using a reversed
967 phase C8 column and pyridine-containing mobile phases. *Mar. Ecol. Prog. Ser.*,
968 195, 29–45.

969

970 Zhou, M., Niiler, P.P. & Hu, J. (2002) Surface currents in the Bransfield and
971 Gerlache Straits, Antarctica. *Deep-Sea Res. Part I Oceanogr. Res. Pap.*, 49,
972 267–280.

973

974 **Acknowledgements**

975 This is a multidisciplinary study as part of the Brazilian High Latitude
976 Oceanography Group (GOAL) activities in the Brazilian Antarctic Program
977 (PROANTAR). Financial support was provided by National Council for Research
978 and Development (CNPq) and Coordination for the Improvement of Higher
979 Education Personnel (CAPES). This study was conducted within the activities of
980 the INTERBIOTA, NAUTILUS, PROVOCCAR, ECOPELAGOS (CNPq grant
981 numbers 407889/2013-2, 405869/2013-4, 442628/2018-8, 442637/2018-7,
982 respectively) and CMAR2 (CAPES grant number 23038.001421/2014-30)
983 projects. The authors thank to the crew of the RV Almirante Maximiano of the
984 Brazilian Navy and several scientists and technicians participating in the cruise
985 for their valuable help during sampling. We are grateful to Simon Wright, from the
986 Australian Antarctic Division, for providing the CHEMTAX v.1.95 software; and
987 Ricardo Pollery, from Federal University of Rio de Janeiro, for performing the
988 nutrient analysis. A MSc fellowship from CAPES was granted to R.R. Costa. A.
989 Ferreira received a PhD grant from Fundação para a Ciência e a Tecnologia
990 (FCT; grant no SFRH/BD/144586/2019). C.R.B. Mendes, R. Kerr and E.R. Secchi
991 are granted with research fellowships from the CNPq. M.S.S. is granted with a
992 PNPd-CAPES fellowship (88882.314596/2019-01). A.C. Brito was funded by

993 FCT through the Scientific Employment Stimulus Programme
994 (CEECIND/0095/2017). Additional support from the FCT was also given to this
995 study (UIDB/MAR/04292/2020; LA/P/0069/2020). CAPES also provided free
996 access to many relevant journals through the portal “Periódicos CAPES”. This
997 study is within the scope of two Projects of the Institutional Internationalization
998 Program (CAPES PrInt-FURG –Edital 41/2017). This research is also framed
999 within the College on Polar and Extreme Environments (Polar2E) of the University
1000 of Lisbon.

1001

1002 **Author contributions**

1003 R.R.C. and C.R.B.M. contributed to the conception and design of this work.
1004 C.R.B.M., M.S.S and R.K. carried out the collection of in situ data. R.R.C. and
1005 C.R.B.M. carried out the HPLC/CHEMTAX analyses. R.R.C. and A.F. performed
1006 the remote sensing analysis. T.S.D. performed the physical oceanography
1007 analysis. M.S.S. carried out the macroscopy analysis. R.R.C. wrote the first draft
1008 of the manuscript and developed the figures. A.F., M.S.S., R.K., T.S.D., V.M.T,
1009 A.C.B, V.B., E.S. and C.R.B.M contributed to the organization and writing of the
1010 final version of the manuscript. All authors contributed to manuscript revision,
1011 read, and approved the submitted version.

1012

1013

1014

1015

1016

1017 **Table 1** | Generalized linear models applied to the biomass of phytoplankton
1018 groups as a function of environmental parameters along the NAP summer
1019 (February and March). Biomass of centric diatoms ($10^7 \mu\text{m}^3 \text{L}^{-1}$), pennate diatoms
1020 ($10^7 \mu\text{m}^3 \text{L}^{-1}$), dinoflagellates ($\text{mg m}^{-3} \text{Chl-a}$), cryptophytes ($\text{mg m}^{-3} \text{Chl-a}$) and
1021 mixed flagellated ($\text{mg m}^{-3} \text{Chl-a}$) is modelled as a function of surface *in situ*
1022 temperature ($^{\circ}\text{C}$), surface *in situ* salinity, mixed layer depth (MLD; m), dissolved
1023 inorganic nitrogen (DIN; μM), grazing index (%) and senescence index (%).
1024 Surface *in situ* salinity did not show any relationship with biomass of
1025 phytoplankton groups and was not selected by AIC, thus not being included in
1026 Table 1. The black solid lines indicate that a given environmental parameter is
1027 not contributing to explain the biomass of a group. Number of samples (n), Akaike
1028 Information Criterion (AIC) and pseudo- R^2 are shown. (*) and (**) indicate
1029 environmental parameters that are statistically significant at $p < 0.1$ and $p < 0.05$,
1030 respectively. Scatter plot of individual relationship between the physical-biological
1031 parameters selected by AIC and biomass of phytoplankton groups is shown in
1032 Supplementary Fig. 9.

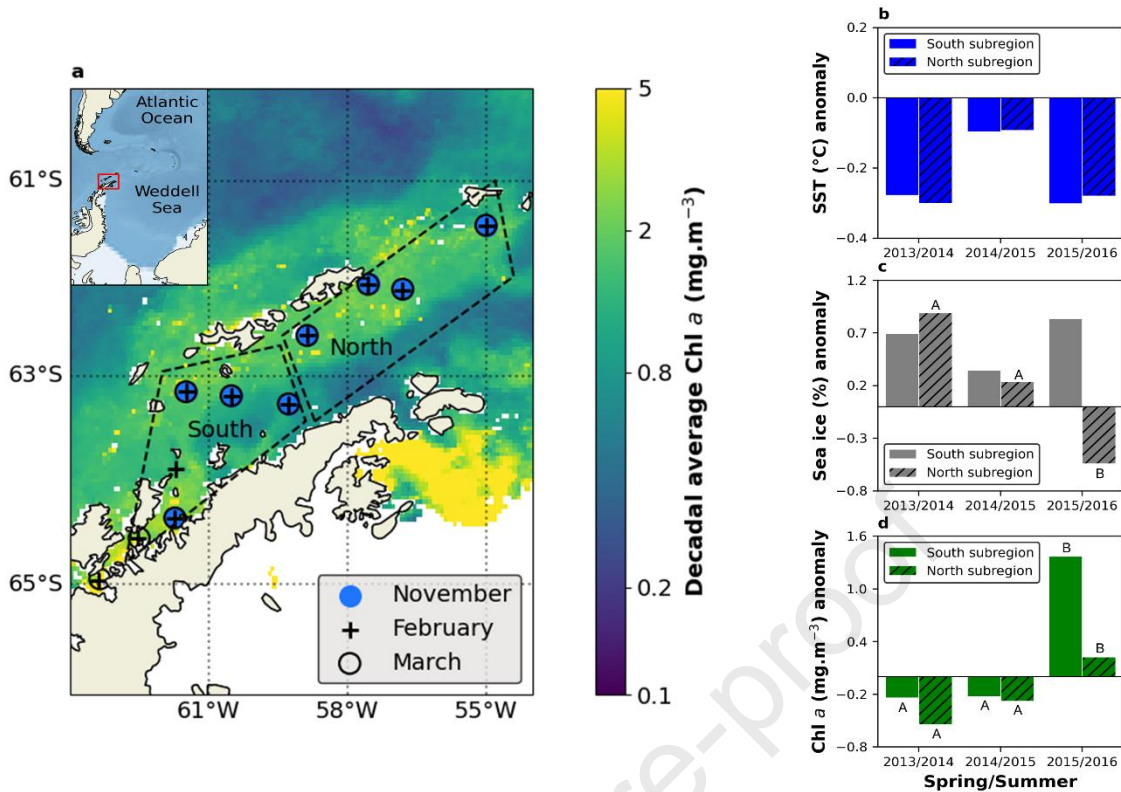
1033

1034

1035

1036

Groups	Temperature	MLD	DIN	Grazing	Senescence	n	AIC	Pseudo-R ²
Centric diatoms	—	0.07 **	0.13 **	—	-0.79 *	60	1062.3	0.5
Pennate diatoms	0.83 **	-0.01	-0.11 **	0.19 *	—	60	1127.1	0.3
Dinoflagellates	—	0.02 *	0.18 **	—	—	83	-65.3	0.7
Cryptophytes	-0.71 **	-0.01	-0.05 **	-0.37 **	—	88	9.8	0.4
Mixed flagellates	—	0.01 *	—	—	0.03	88	-160.9	0.1



1

2 **Figure 1** | Study area and remote sensing measurements.(a) Locations of
 3 stations are presented by blue circles (November), black pluses (February) and
 4 open circles (March). Subregions (south and north) are presented by the black
 5 dashed lines, which delimited the areas used to estimate average remote sensing
 6 measurements. The decadal-mean (2010–2019) remote sensing chlorophyll-a
 7 (Chl-a) during the spring/summer (November–March) is represented by the color
 8 scale bar on the right and exhibited in the background, indicating phytoplankton
 9 biomass (Chl-a) distribution along the NAP over the past decade. An inset map
 10 in the upper left corner shows the location of the NAP within the Atlantic sector of
 11 the Southern Ocean. Anomalies of (b) sea surface temperature (SST), (c) sea ice
 12 fraction and (d) Chl-a relative to the decadal average during the spring/summer
 13 of 2013/2014, 2014/2015 and 2015/2016 along the south (filled bar) and north
 14 (dashed bar) subregions of the NAP.(b–d) ANOVA test was applied to measure

15 differences among groups in each subregion (i.e., if there are spring/summer
16 differences in parameters within each subregion). The capital letters indicate
17 statistical groupings, which differ each other at $p < 0.05$, based on Tukey test.
18 Note that the tests of hypothesis were applied considering differences between
19 spring/summer periods and the results (showed by capital letters) are
20 represented along with the anomalies relative to the decadal average. In (a), $n =$
21 1512. In (b-d), $n = 151, 151$ and 152 for 2013/2014, 2014/2015 and 2015/2016,
22 respectively.

23

24

25

26

27

28

29

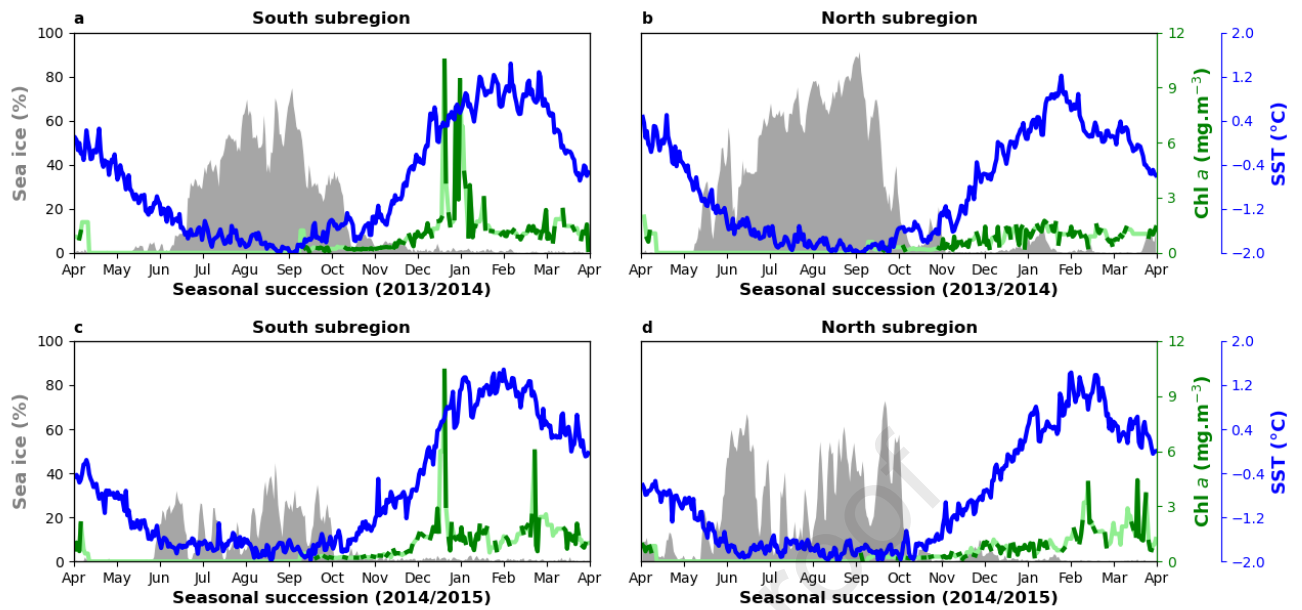
30

31

32

33

34



35

36 **Figure 2** | Seasonal variability in remote sensing measurements.(a–d) Sea ice
 37 fraction (gray area), sea surface temperature (SST, solid blue line) and
 38 chlorophyll-a (Chl-a, solid green line) during the seasonal succession periods of
 39 2013/2014 and 2014/2015 along the south and north subregions of the NAP. The
 40 solid light green lines represent Chl-a linearly interpolated values.

41

42

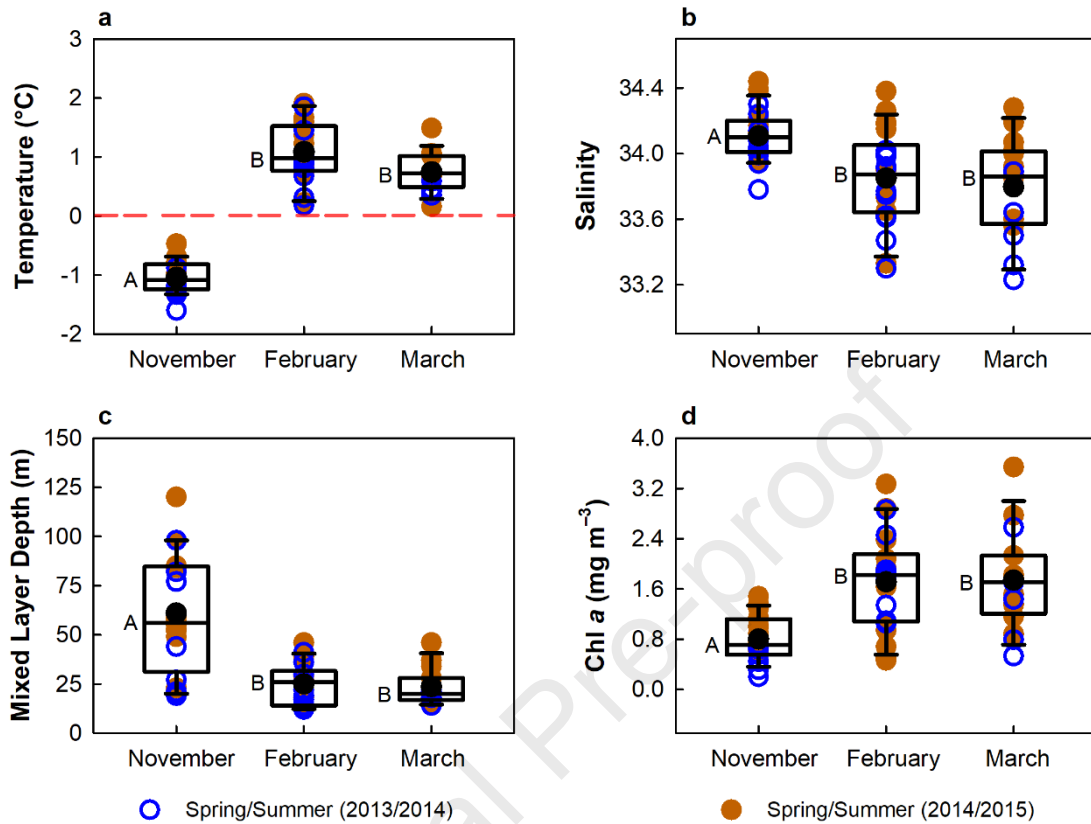
43

44

45

46

47



48

49 **Figure 3** | Physical parameters and Chl-a over the phytoplankton seasonal
 50 succession. (a) *In situ* surface temperature, (b) surface salinity, (c) mixed layer
 51 depth (MLD) and (d) chlorophyll-a (Chl-a) during the late spring (November) and
 52 summer months (February and March). Blue open circles and brown circles
 53 represent individual values to the spring/summer (November, February and
 54 March) of 2013/2014 and 2014/2015, respectively. (a) The horizontal dashed red
 55 line represents a marked segregation between the late spring and summer
 56 months according to the *in situ* surface temperature, which is additionally
 57 investigated in Figure 4. The horizontal lines of the boxes indicate upwards the
 58 25th, 50th (median) and 75th percentiles, respectively. Average values are
 59 represented by black circles. The whiskers extend to values not considered as

60 outliers. Kruskal–Wallis test was applied to measure differences among groups
61 (i.e., months), considering the same month (November, February or March) as a
62 sole grouping (see “Methods”) (a: $H = 44.2$, $p < 0.001$; b: $H = 16.0$, $p < 0.001$; c:
63 $H = 21.1$, $p < 0.001$; d: $H = 21.8$, $p < 0.001$). The capital letters indicate statistical
64 groupings, which differ each other at $p < 0.05$, based on all pairwise multiple
65 comparison procedures with Dunn’s Method. In (a–d), $n = 23$, 22 and 16 for
66 November, February and March, respectively.

67

68

69

70

71

72

73

74

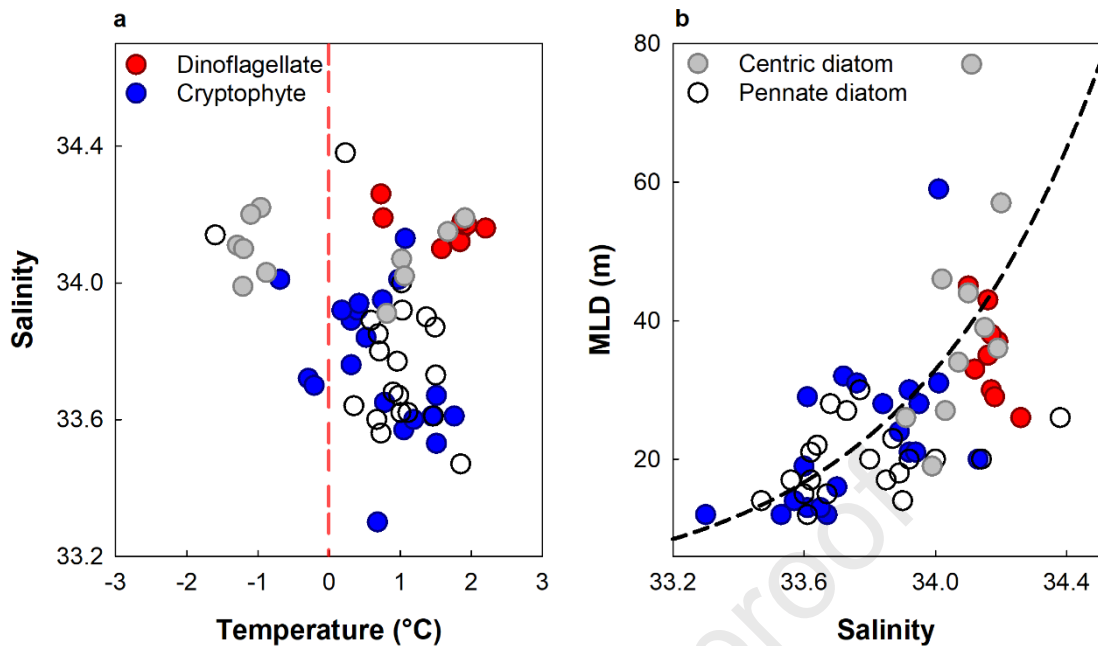
75

76

77

78

79



80

81 **Figure 4** | Distribution of phytoplankton groups driven by physical parameters.

82 High proportion (> 45% to the total Chl-a) of dinoflagellates (red circles; n = 10),

83 cryptophytes (blue circles; n = 20) and diatoms (centric – gray circle, n = 11; and

84 pennate – black open circle, n = 20) relative to the (a) *in situ* surface temperature

85 versus surface salinity and (b) surface salinity versus mixed layer depth (MLD)

86 during the late spring (November) and summer months (February and March).

87 High proportion of centric or pennate diatoms was measured according to the cell

88 density > 50% in relation to the total diatom abundance, counted by microscopy

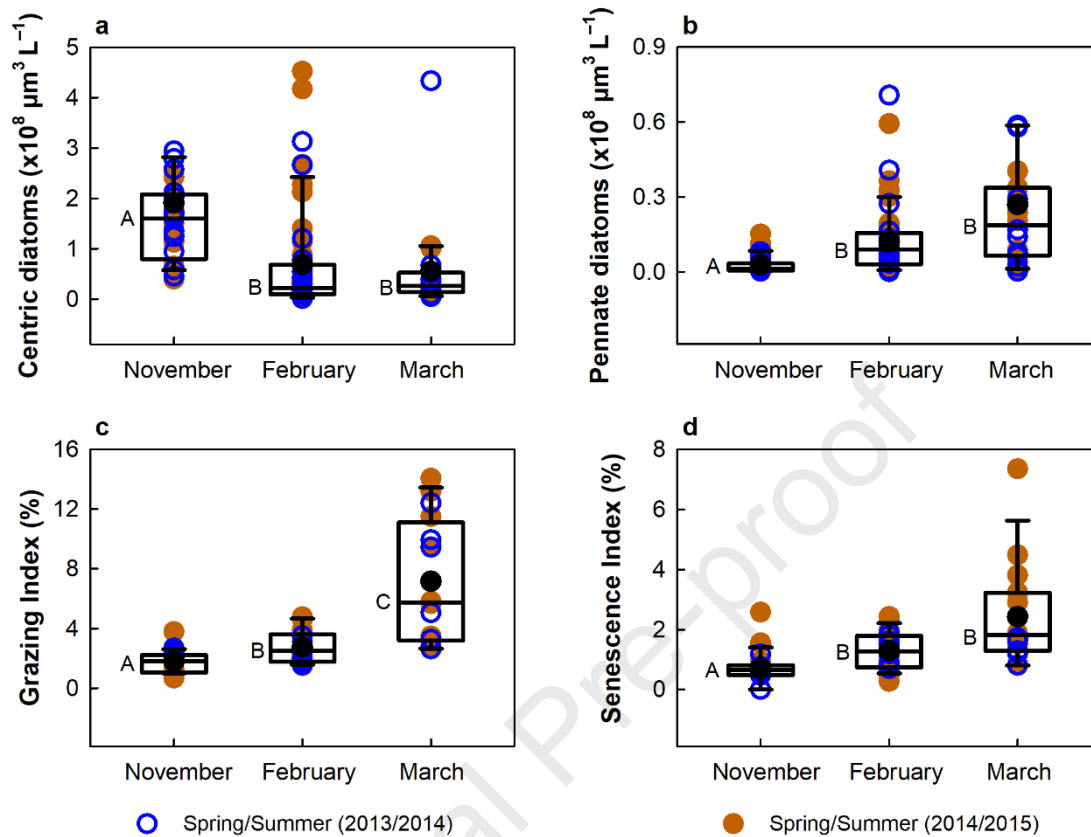
89 analysis, in those stations by which diatom proportion was > 45% to the total Chl-

90 a via HPLC/CHEMTAX analysis. (a) The dashed red line represents a clear *in situ*

91 surface temperature difference between the late spring and summer, such as

92 observed in Figure 3a. (b) The dashed black line shows the relationship ($R^2 = 0.4$,93 $p < 0.0001$, and $n = 61$) between surface salinity and MLD.

94



95

96 **Figure 5** | Centric and pennate diatoms and biotic parameters over the
 97 phytoplankton seasonal succession. (a) Centric and (b) pennate diatoms, and (c)
 98 grazing and (d) senescence indices during the late spring (November) and
 99 summer months (February and March). Blue open circles and brown circles
 100 represent individual values to the spring/summer (November, February or March)
 101 of 2013/2014 and 2014/2015, respectively. The horizontal lines of the boxes
 102 indicate upwards the 25th, 50th (median) and 75th percentiles, respectively.
 103 Average values are represented by black circles. The whiskers extend to values
 104 not considered as outliers. Kruskal–Wallis test was applied to measure
 105 differences among groups (i.e., months), considering the same month
 106 (November, February or March) as a sole grouping (see “Methods”) (a: $H = 39.7$,

107 $p < 0.001$; b: $H = 35.6$, $p < 0.001$; c: $H = 32.0$, $p < 0.001$; d: $H = 20.9$, $p < 0.001$).
108 The capital letters indicate statistical groupings, which differ each other at $p <$
109 0.05 , based on all pairwise multiple comparison procedures with Dunn's Method.
110 In (a-d), $n = 23$, 22 and 16 for November, February and March, respectively.

111

112

113

114

115

116

117

118

119

120

121

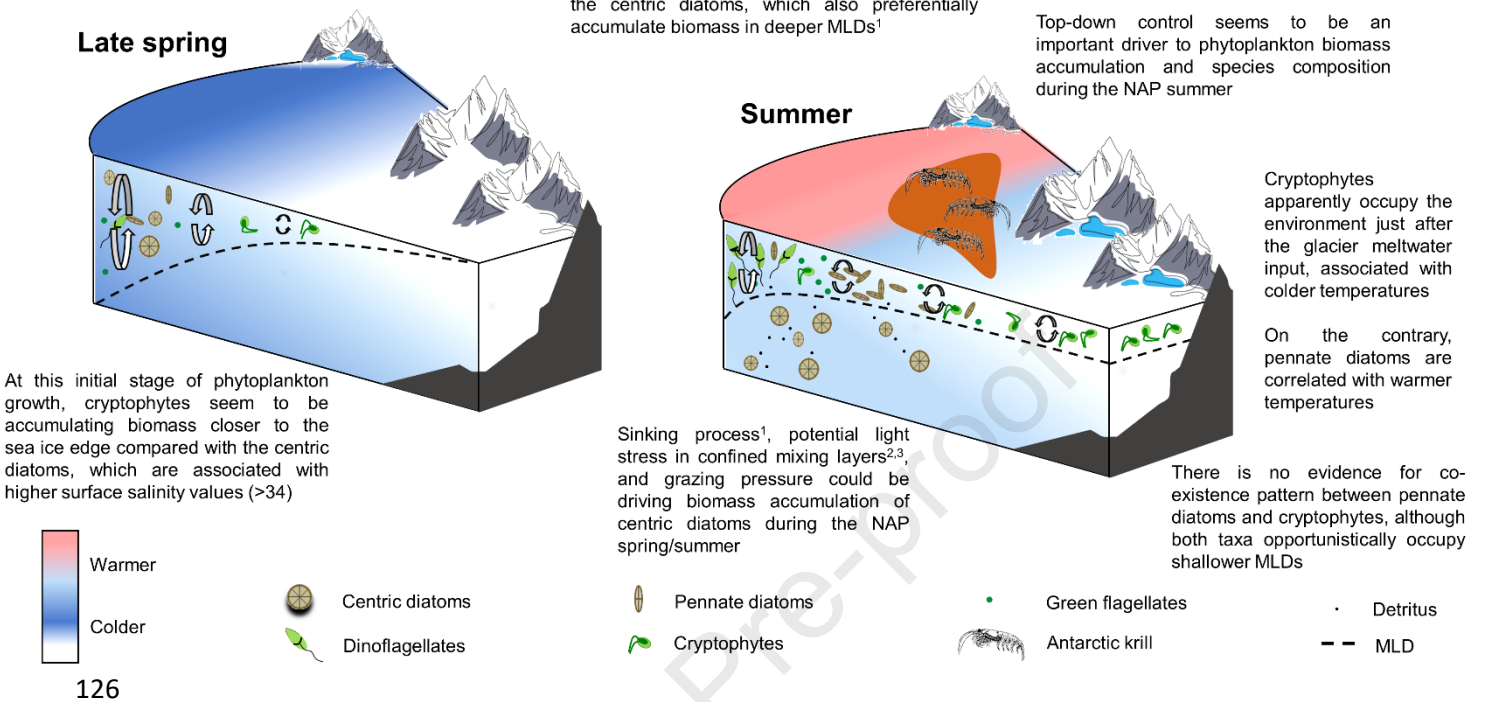
122

123

124

125

Phytoplankton community composition is highly homogeneous during the spring compared with the NAP summer, when the major taxa accumulate biomass



127 **Figure 6** | Illustration of physical-biological drivers modulating phytoplankton
 128 seasonal succession along the NAP. The schematic figure shows the late spring,
 129 characterized by a highly homogeneous distribution of phytoplankton groups (i.e.,
 130 no bloom formation), and the summer when pennate diatoms, cryptophytes or
 131 dinoflagellates dominate phytoplankton community composition in the NAP
 132 marine environment, as large centric diatoms leave the upper ocean system. This
 133 illustration is based on analysis of this study and references, as following: (1)
 134 Costa et al. 2021; (2) Petrou et al. 2016; and (3) Mendes et al. 2023.

135

Groups	Temperature	MLD	DIN	Grazing	Senescence	n	AIC	Pseudo-R ²
Centric diatoms	—	0.07 **	0.13 **	—	-0.79 *	60	1062.3	0.5
Pennate diatoms	0.83 **	-0.01	-0.11 **	0.19 *	—	60	1127.1	0.3
Dinoflagellates	—	0.02 *	0.18 **	—	—	83	-65.3	0.7
Cryptophytes	-0.71 **	-0.01	-0.05 **	-0.37 **	—	88	9.8	0.4
Mixed flagellates	—	0.01 *	—	—	0.03	88	-160.9	0.1

Highlights

Spring/summer sea ice melt enhances stratification, fuelling phytoplankton growth

Grazing activity may control phytoplankton development during spring/summer

Cryptophytes and pennate diatoms preferentially occupy shallower mixing layers

Pennate and centric diatoms exhibit a distinct fundamental niche

Different strategies of phytoplankton groups modulate their seasonal succession

Declaration of interests

The authors declare that they have no known competing financial interests or personal relationships that could have appeared to influence the work reported in this paper.

The authors declare the following financial interests/personal relationships which may be considered as potential competing interests:

Journal Pre-proof